Published online 5 November 2018

Nucleic Acids Research, 2019, Vol. 47, No. 2 ***899–910***
doi: 10.1093/nar/gky1089

Dynamic protein–RNA interactions in mediating splicing catalysis

Che-Sheng Chung[1,†], Chi-Kang Tseng[1,†], Yung-Hua Lai[1,2], Hui-Fang Wang[1,2], Andrew J. Newman[3] and Soo-Chen Cheng[1,*]

[1]Institute of Molecular Biology, Academia Sinica, Taipei, Taiwan 115, Republic of China, [2]Department of Life Sciences and Institute of Genome Sciences, National Yang-Ming University, Taipei, Taiwan 112, Republic of China and [3]MRC Laboratory of Molecular Biology, Francis Crick Avenue, Cambridge CB2 0QH, UK

Received September 05, 2018; Revised October 07, 2018; Editorial Decision October 11, 2018; Accepted October 19, 2018

ABSTRACT

The spliceosome is assembled via sequential interactions of pre-mRNA with five small nuclear RNAs and many proteins. Recent determination of cryo-EM structures for several spliceosomal complexes has provided deep insights into interactions between spliceosomal components and structural changes of the spliceosome between steps, but information on how the proteins interact with pre-mRNA to mediate the reaction is scarce. By systematic analysis of proteins interacting with the splice sites (SSs), we have identified many previously unknown interactions of spliceosomal components with the pre-mRNA. Prp8 directly binds over the 5′SS and the branch site (BS) for the first catalytic step, and the 5′SS and 3′SS for the second step. Switching the Prp8 interaction from the BS to the 3′SS requires Slu7, which interacts dynamically with pre-mRNA first, and then interacts stably with the 3′-exon after Prp16-mediated spliceosome remodeling. Our results suggest that Prp8 plays a key role in positioning the 5′SS and 3′SS, facilitated by Slu7 through interactions with Prp8 and substrate RNA to advance exon ligation. We also provide evidence that Prp16 first docks on the intron 3′ tail, then translocates in the 3′ to 5′ direction on remodeling the spliceosome.

INTRODUCTION

Pre-mRNA splicing proceeds *via* a two-step transesterification reaction. The reaction is catalyzed by the spliceosome, which is assembled by sequential binding of five snRNAs and numerous protein factors to the pre-mRNA (1–3). During spliceosome assembly, U1 and U2 bind to the 5′ splice site (5′SS) and the branch site (BS), respectively, and form base pairs with the conserved splice site sequence to form the prespliceosome. Following binding of the U4/U6.U5 tri-snRNP, the spliceosome undergoes a dramatic structural rearrangement, releasing U1 and U4, and forming new base pairs between U2 and U6, and U6 and the 5′ splice site, to form the activated spliceosome.

RNA base pairings play roles in the recognition of splice sites by snRNAs, and also form the framework of the catalytic center of the active spliceosome. The structure is stabilized by protein factors. While components of U1 and U2 snRNPs play roles in stabilizing the interaction of U1 and U2 with the pre-mRNA, a protein complex associated with Prp19, named the NineTeen complex (NTC), is required for stabilizing the association of U5 and U6 with the spliceosome by promoting specific interaction of U5 and U6 with the pre-mRNA during spliceosome activation (4). NTC remains stably associated with the spliceosome until completion of the reaction, and can serve as a marker for post-activation spliceosomes (5,6).

Structural changes of the spliceosome are mediated by members of the DExD/H-box RNA helicase family, which utilize energy from ATP hydrolysis to unwind RNA duplexes or to remodel ribonucleoprotein complexes (7,8). Two DExD/H-box proteins, Prp2 and Prp16, are required during the catalytic phase. After activation of the spliceosome, Prp2 promotes destabilization of the U2 component SF3a/b (9,10) to allow binding of Cwc25, which is required for the first reaction (9,11). Cwc25 becomes stably associated with the spliceosome after the reaction, and requires Prp16 for its displacement before the second reaction can take place (12). Another protein factor, Yju2, which is required for the recruitment of Cwc25 to the spliceosome, is also displaced (12,13). After the removal of Yju2 and Cwc25, Slu7 and Prp18 are required to promote the second reaction (12). Upon completion of the reaction, mature mRNA is first released from the spliceosome, catalyzed by Prp22 (14), and the spliceosome is then disassembled into its separate components. In the yeast *Saccharomyces cere-*

*To whom correspondence should be addressed. Tel: +886 2 27899200; Fax: +886 2 27883296; Email: mbscc@ccvax.sinica.edu.tw
Present address: Chi-Kang Tseng and Hui-Fang Wang, Institute of Molecular Biology, 55128 Mainz, Germany
†The authors wish it to be known that, in their opinion, the first two authors should be regarded as Joint First Authors.

visiae, disassembly of the spliceosome is mediated by the NTR protein complex, comprising Ntr1, Ntr2, Cwc23 and the DEAH-box protein Prp43 (15–18).

Recent determination of cryo-EM structures for several spliceosomal complexes has revealed the arrangement of protein and RNA components on spliceosomes at different catalytic stages (19–31), but provided little information on how protein components mediate positioning of the 3′ splice site (3′SS) for exon ligation since only limited pre-mRNA sequence was observed. By systematic site-specific crosslinking analysis of proteins to RNA sequences across the splice sites for spliceosomes arrested at specific stages of the splicing pathway, we were able to elucidate changes in protein–RNA interactions along the pathway. Most of the proteins binding around the 5′SS do not significantly change their interaction modes throughout the catalytic phase. Prp8 was seen to crosslink to the 5′-exon near the splice junction, and Snu114, Cwc22 and Cwc21 crosslinked to positions further upstream at around position $-20^{5'SS}$. Proteins crosslinked to the intron sequences include Cwc2, Ecm2 and several NTC components. By contrast, proteins that bind to the BS-3′SS region show substantial changes between steps. On the B^{act} complex, U2 component Hsh155 was seen to crosslink across the BS. After Prp2-mediated remodeling of the spliceosome, Prp8 replaces Hsh155 to crosslink across the BS, but switches its interaction to the 3′SS after Prp16-mediated spliceosome remodeling. Our results show that Prp8 directly binds over the 5′SS and the BS during the first catalytic step, and over the 5′SS and 3′SS during the second step. Step one factor Cwc25 only crosslinked to the BS downstream region during the first step, and step two factors Slu7 and Prp22 crosslinked to both the intron and 3′-exon flanking the Prp8 crosslinked site. We also found that Slu7 dynamically interacts with the intron 3′ tail (i3′T) after Prp2-mediated spliceosome remodeling and throughout the catalytic phase. Such interactions might facilitate positioning of the 3′SS at the active site for exon ligation. Our results suggest that Prp8 is the key player in positioning the splice sites to promote catalysis, while step one and step two factors facilitate or stabilize the interactions of Prp8 with the splice sites to promote the reactions.

MATERIALS AND METHODS

Yeast strains

The following yeast strains were used:

BJ2168 MATa prc1 prb1 pep4 leu2 trp1 ura3
YSCC024 MATa prc1 prb1 pep4 leu2 trp1 ura3 HSH155-HA
YSCC22 MATa prc1 prb1 pep4 leu2 trp1 ura3 PRP22–4V5
YSCC25 MATa prc1 prb1 pep4 leu2 trp1 ura3 CWC25-HA
YSCC701 MATa prc1 prb1 pep4 leu2 trp1 ura3 SLU7-V5
YSCC8–1 MATa prc1 prb1 pep4 leu2 trp1 ura3 LEU2::GAL1-PRP8, pRS314.PRP8.ZZ.TEV970
YSCC8–2 MATa prc1 prb1 pep4 leu2 trp1 ura3 LEU2::GAL1-PRP8, pRS314.PRP8.ZZ.TEV1281
YSCC8–3 MATa prc1 prb1 pep4 leu2 trp1 ura3 LEU2::GAL1-PRP8, pRS314.PRP8.ZZ.TEV1413
YSCC8–4 MATa prc1 prb1 pep4 leu2 trp1 ura3 LEU2::GAL1-PRP8, pRS314.PRP8.ZZ.TEV1503
YSCC8–5 MATa prc1 prb1 pep4 leu2 trp1 ura3 LEU2::GAL1-PRP8, pRS314.PRP8.ZZ.TEV1673

Antibodies and reagents

Anti-V5 antibody was purchased from Serotec Inc. Anti-HA antibody was produced by immunizing mice with a keyhole limpet hemocyanin (KLH)-conjugated HA peptide (unpublished). Anti-Prp16, anti-Prp22, anti-Prp8, anti-Ntc20, anti-Yju2, anti-Cwc2 and anti-Cwc25 polyclonal antibodies were produced by immunizing rabbits with fragments or full-length recombinant Prp16 (1-298), Prp22 (1-484), Prp8 (1-115), Ntc20, Yju2, Cwc2 and Cwc25 proteins, respectively. Dinucleotide 4-thio-UpG was purchased from Dharmacon. SP6 RNA polymerase was purchased from Promega, RNase P1 from Sigma, and RNasin and T4 RNA ligase 2 from Enzymatics. Protein A-Sepharose CL-4B and IgG Sepharose were purchased from GE Healthcare. Complete, EDTA-free Protease Inhibitor Cocktail was purchased from Roche. TEV protease with a mutation (Ser219Asn) at the internal self-cleavage site was a kind gift of Hung-Ta Chen (Institute of Molecular Biology, Academia Sinica).

Splicing extracts and substrates

Splicing extracts were prepared according to Cheng *et al.* (32). The pre-mRNA substrates were prepared by *in vitro* transcription with SP6 RNA polymerase. *Eco*RI-linearized pSP64–88 plasmid was used as the template for preparation of regular actin substrate. We adapted the method of Sontheimer for preparation of 4sU-labeled pre-mRNA substrates (33). DNA templates were generated by polymerase chain reaction (PCR) using pSP64–88 plasmid as a template. Primers used for PCR are listed in Supplemental Table S1. For preparation of the 5′ RNA fragment, transcription reactions were performed in 40 mM Tris–HCl (pH 7.9), 6 mM $MgCl_2$, 2 mM spermidine, 10 mM NaCl, 10 mM DTT, 2 units/μl RNasin, 0.5 mM each of the four NTPs, 6.6 nM of α-^{32}P-UTP (3000 Ci/mmole), 60 nM DNA template and 1.9 units/μl SP6 RNA polymerase. For preparation of the 3′ fragment, transcription reactions were performed under the same conditions with the addition of 2.5 mM 4sUpG dinucleotide. The RNA fragments were all purified by electrophoresis on 5% polyacrylamide gels. The 3′ fragment was phosphorylated with ^{32}P at the 5′-end using T4 polynucleotide kinase in a 10 μl reaction containing 2 μM of the RNA fragment. For ligation of the 5′ and 3′ fragments, 10 μl of the phosphorylated 3′ fragment was mixed with 10 μl of 6 μM 5′ fragment, 1.25 μl of 32 μM DNA splint, and 2.5 μl of 1M Tris–HCl (pH 7.4) to make a final volume of 24 μl. Pre-mRNA with 4sU labeled at the $+4^{5'SS}$ position was generated by 3-fragment-ligation of the 5′ fragment, RNA oligo R2 and the 3′ fragment together with the DNA splint at a ratio of 4:2:4:3. The mixtures were incubated at 65°C for 20 min, shifted to 37°C for 15 min, and then 25°C for 20 min. After addition of 11.5 μl dH_2O, 1.25 μl of 16 mM ATP, 7.5 μl of 50% PEG-8000, 1 μl of RNasin, and 5 μl of T4 RNA ligase 2, the mixtures were incubated at 37°C for 2 h. The ligated products were purified by electrophoresis on 5% denaturing polyacrylamide gels.

Immunoprecipitation and immunodepletion

Immunoprecipitation of the spliceosome was performed as described (5). For each 10–20 μl of splicing reaction mixtures, 10 μl of protein A-Sepharose (PAS) conjugated with 1.5 μl of anti-Ntc20 antibody or 5 μl of anti-Prp16 antibody was used. For precipitation of the Slu7-V5- or Cwc25-HA-associated spliceosome, 1 μl of anti-V5 antibody or 15 μl of anti-HA antibody was used, respectively. For depletion of specific proteins from 100 μl of yeast extracts, 12.5 mg of PAS was swollen in NET-2 buffer (50 mM Tris–HCl, pH 7.4, 150 mM NaCl, 0.05% NP-40) to make a bed volume of 50 μl, and this was used for conjugation with specific antibodies. For depletion of Prp16, Spp2 and Yju2, 50 μl of anti-Prp16, 200 μl of anti-Spp2 and 120 μl of anti-Yju2 antibodies were used, respectively. For co-depletion of Slu7 and Prp22, 50 μl of anti-Slu7 antiserum and 1.3 μg of purified anti-Prp22 antibody were used. Each 100 μl of extracts was incubated with antibody-conjugated PAS at 4°C for 1 h, and supernatants were collected as depleted extracts.

Crosslinking analysis

Splicing reactions were carried out with 0.4 nM of 4sU-labeled actin pre-mRNA in the presence of 0.4 U/μl RNasin. The reaction mixtures were spread onto a piece of parafilm overlaid on an ice-cold aluminum block and irradiated with UV_{365nm} for 10 min at a distance of ∼2 cm using a hand UV Lamp (Model UVGL-25, UVP Inc.). Spliceosomes were incubated with specific antibodies conjugated to protein A-Sepharose. The precipitated spliceosomes were incubated at 37°C for 30 min following addition of an equal volume of solution containing 0.06 U/μl RNase P1 and 6× Complete, EDTA-free Protease Inhibitor Cocktail (2X P1/CPI) before analyzing on SDS-PAGE. For immunoprecipitation of specific proteins, splicing reaction mixtures were treated with P1/CPI as described above, and then denatured by heating at 100°C for 1.5 min in 1% SDS (w/v), 1% Triton X-100 (v/v) and 100 mM DTT. After centrifugation to remove insoluble materials, the mixtures were diluted 10-fold with a cold buffer containing 50 mM Tris–HCl (pH 7.5), 300 mM NaCl and 0.05% NP-40, and subjected to immunoprecipitation. The precipitates were treated with P1/CPI, and then analyzed by SDS-PAGE.

Mapping of crosslinked sites on Prp8

Splicing was carried out in extracts prepared from ZZ-tagged Prp8 strains with a TEV cleavage site inserted at various positions (34) using actin ACAC pre-mRNA with 4sU-labeled at the +8 or +37 position of the branch site. Following UV irradiation and P1/CPI treatment, Prp8 was pulled-down with a $\frac{1}{2}$ volume of IgG-Sepharose. The precipitates were washed three times with NET-2 buffer and once with NET-2 supplemented with 5 mM DTT, and then incubated at 18°C for 30 min upon addition of 0.4 μg TEV protease per 10 μl beads. The precipitates were further treated with P1/CPI and washed four times with a buffer containing 50 mM Tris–HCl (pH 7.4), 300 mM NaCl, 0.1% SDS and 0.1% Triton X-100 before fractionation by 6% SDS-PAGE.

RESULTS

To understand how proteins mediate structural changes of the spliceosome through interactions with pre-mRNA, we systematically analyzed crosslinking of proteins to the pre-mRNA at various stages of the splicing cycle. Splicing was arrested at different stages by depletion of specific factors from splicing extracts in the following ways: (i) depletion of Spp2 for post-activation (B^{act}); (ii) depletion of Yju2 for the pre-catalytic stage (B^{*}); (iii) depletion of Prp16 for post-first-reaction (C); (iv) adding dominant-negative Prp16 mutant D473A protein to the splicing reaction for the Prp16-associated spliceosome (C1) (12,35); (v) using 3′ splice site mutant ACAC pre-mRNA for pre-second-reaction (C^{*}) and (vi) adding dominant-negative Prp22 mutant S635A protein to the splicing reaction for post-second-reaction (P) (36–38) (Figure 1). Actin pre-mRNAs were synthesized with a single nucleotide being replaced with 4-thiouridine (4sU) for several positions around the 5′SS, BS and 3′SS. Substrates were prepared in such a way that each pre-mRNA molecule contained only one ^{32}P at the 5′-end of the 4sU residue, ensuring that the crosslinked proteins would be labeled with ^{32}P after digestion of crosslinked products with RNase P1. Several transcripts had one or two downstream nucleotides also changed to purines to increase the yields of transcripts synthesized by SP6 RNA polymerase (Supplementary Figure S1). Splicing reaction mixtures were irradiated with UV_{365nm}, and then precipitated with specific antibodies. After RNase P1 treatment, total precipitated proteins were analyzed by SDS-PAGE. To identify specific crosslinked proteins, reaction mixtures were first treated with RNase P1 following UV-irradiation, and then treated with denaturant before immunoprecipitation (Figure 2A). A summary of the results is shown in Figure 2B.

Identification of proteins crosslinked to the intron 3′ tail during the first catalytic step

The B^{act} complex was isolated using anti-HA antibody by assembling the spliceosome in Spp2-depleted Hsh155-HA extracts. Hsh155 was seen to crosslink across the branch-point (Figure 3A and Supplementary Figure S2A), and the pre-mRNA retention and splicing complex (RES) components, Bud13, Pml1 and Snu17, crosslinked in the downstream region between positions $+22^{BS}$ to $+37^{BS}$ (Figure Supplementary Figure S2B), in agreement with previous reports (39–41). A strong crosslink from the $+18^{BS}$ position toward the 3′SS of an unidentified protein of around 65-kD was also seen in the B^{act} complex, and persisted through the first step (see below). A major change in the crosslinking pattern was seen after Prp2-mediated remodeling of the spliceosome due to the release of the SF3 and RES complexes. In the B^{*} complex, isolated by anti-Ntc20 antibody precipitation of spliceosomes assembled in Yju2-depleted extracts, Prp8 replaced Hsh155 to interact with the BS with strong crosslinking at positions $+3^{BS}$ to $+12^{BS}$ (Figure 3B and Supplementary Figure S3A). Prp45 was observed to crosslink at positions $+8^{BS}$ to $+37^{BS}$ in the i3′T (Supplementary Figure S3B). Interestingly, step 2 factors Prp22 and Slu7 were also seen to crosslink to the same region

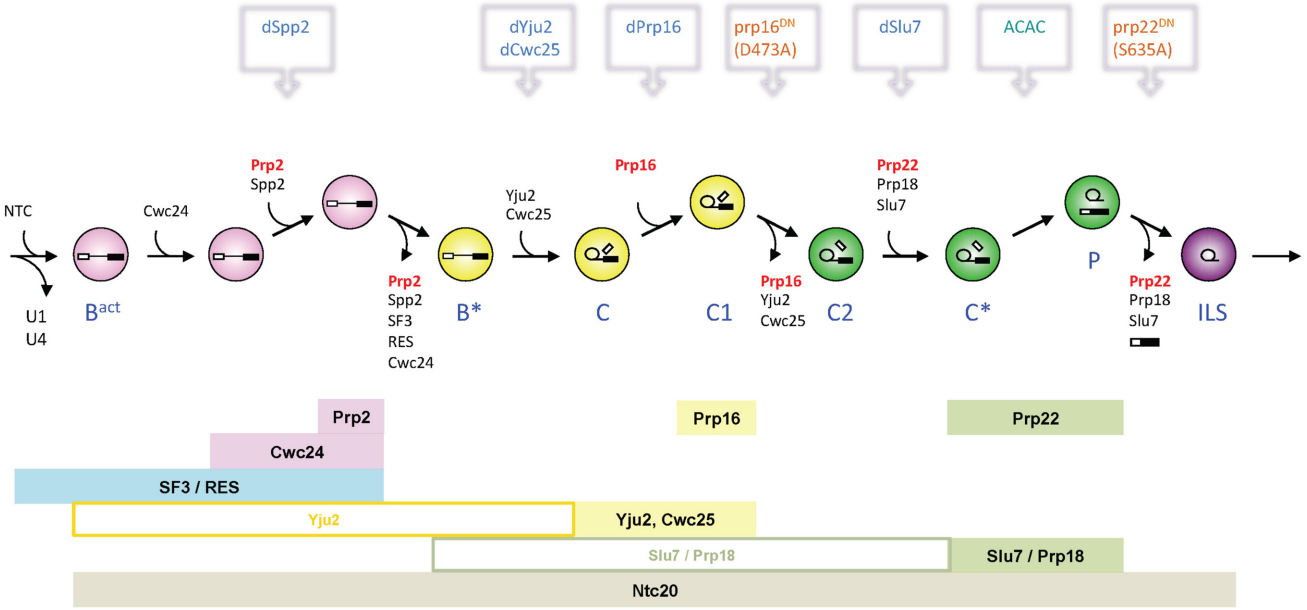

Figure 1. Schematic of the splicing pathway during catalytic steps. Remodeling of the spliceosome mediated by DExD/H-box proteins is indicated by color changes in the spliceosome. Proteins uniquely present in specific complexes are shown below the pathway, with open boxes indicating low-affinity association with the spliceosome. Methods for blocking the pathway at specific steps used in this work are shown above the pathway.

as Prp45 (Supplementary Figure S3B and S3C), indicating that they can enter the spliceosome and contact pre-mRNA at a much earlier stage, i.e., before they are required for action.

After the first reaction, Prp8 continued interacting with the branch site in the absence of Prp16 (as in complex C, Figure 3C and Supplementary Figure S3D), or with Prp16 bound using a dominant-negative D473A mutant (complex named C1, Figure 3D) (35,37), except that crosslinking at the $+3^{BS}$ position was extensively weakened. Prp45 and Slu7 continued interacting with the same region of the i3′T in the C and C1 complexes, but interactions of Prp22 appeared to be excluded from the branch site (Figure 3C and D). We also observed weak crosslinking of Cwc25 at the $+12^{BS}$ and $+18^{BS}$ positions (Supplementary Figure S3D). Cwc25 was previously shown to crosslink to the $+3^{BS}$ position (42), and indeed could be detected to crosslink at the $+3^{BS}$ position on longer exposure of the film. This finding indicates that the primary Cwc25 interacting site is between positions $+12^{BS}$ and $+18^{BS}$. In the C1 complex, Prp16-D473A presented strong crosslinks to the region from position $+18^{BS}$ toward the 3′SS (Figure 3D and Supplementary Figure S3E), which may represent the docking site of Prp16 on the i3′T to mediate the release of Yju2 and Cwc25 from the catalytic center. These data reveal an ordered arrangement of Prp8, Cwc25 and Prp16 interactions with the i3′T.

A Slu7-dependent switch of Prp8 binding site from the BS to the 3′SS prior to exon ligation

The splicing reaction carried out with ACAC pre-mRNA is blocked for the second catalytic reaction, with Slu7/Prp18/Prp22 stably bound to the spliceosome and forming the C^* complex, which represents the structure immediately before exon ligation. The C^* complex was assembled in Prp22-V5 extracts and selected with anti-V5 antibody. Prp8 was found to crosslink near to the 3′SS from positions $+25^{BS}$ to $+37^{BS}$ (Figure 3E, Supplementary Figures S4A and S4B), indicating that Prp8 switched its interaction from the BS to the 3′SS prior to exon ligation. Strong crosslinking of Prp22 at position $+8^{BS}$ and weak crosslinking of Slu7 at $+12^{BS}$ were also detected (Figure 3E and Supplementary Figure S4C). All three proteins continued interacting with the same regions of the i3′T after exon ligation, as observed in the P complex selected with anti-V5 antibody from splicing reactions performed in the presence of V5-tagged Prp22 dominant-negative S635A mutant protein (Figure 3F, Supplementary Figures S4D and E). Unlike at previous stages when several other proteins were also seen to crosslink to the i3′T, only Prp8, Slu7 and Prp22 were detected in the C^* and P complexes, with an additional unidentified 20-kDa protein at position $+25^{BS}$ in the P complex. Prp22 was previously shown to bind to the i3′T after Prp16-mediated remodeling of the spliceosome, and then to translocate to the 3′-exon after exon ligation to promote mRNA release (40,43). However, the excised intron-lariat was still protected from oligo-directed RNase H cleavage (43). Consistently, we found that Prp22, as well as Slu7, continued to interact with the i3′T after exon ligation.

To determine whether Slu7/Prp18/Prp22 are required for switching the Prp8-interacting site, we depleted Slu7 and Prp22 from the extract and isolated the spliceosome with anti-Ntc20 antibody (complex named C2). We found that Prp8 remained interacting with the BS, as in the C complex (Figure 3G), indicating a requirement for Slu7/Prp18/Prp22 to direct Prp8 to the 3′SS. Depletion of Prp22 alone did not prevent crosslinking of Prp8 to the 3′SS (data not shown), suggesting that Slu7 is the major

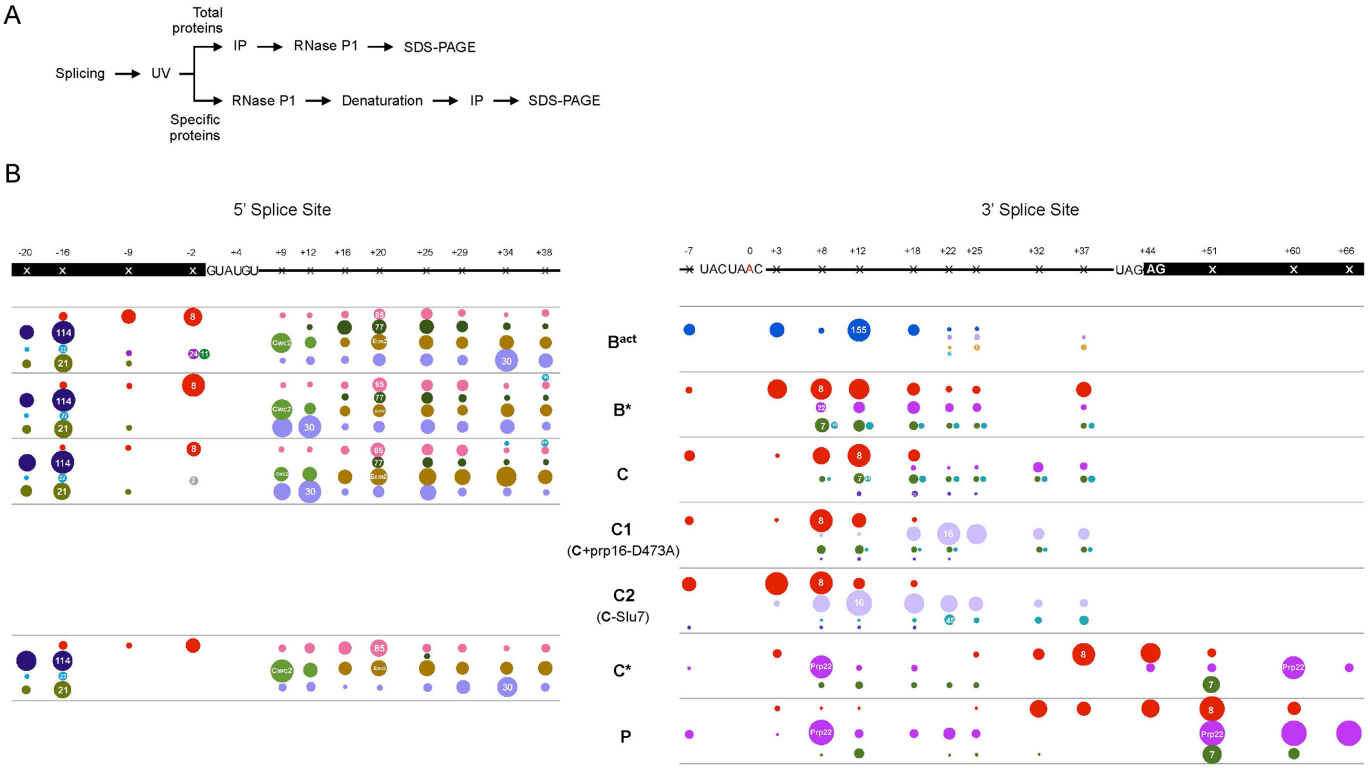

Figure 2. Analysis of total crosslinked proteins in the 5′SS and BS-3′SS regions. (**A**) Procedure of crosslinking analysis. IP, immunoprecipitation. (**B**) Summary of proteins crosslinked to the 5′SS and BS-3′SS regions. The sizes of the circles are representative of the estimated strength of crosslinking signals. 8, Prp8; 114, Snu114; 22, Cwc22; 21, Cwc21; 24, Cwc24; 11, Prp11; 2, Yju2; 85, Ntc85; 77, Ntc77; 30, Ntc30; 90, Ntc90; 155, Hsh155; 13, Bud13; 1, Pml1; 17, Snu17; 25, Cwc25; 16, Prp16; 7, Slu7.

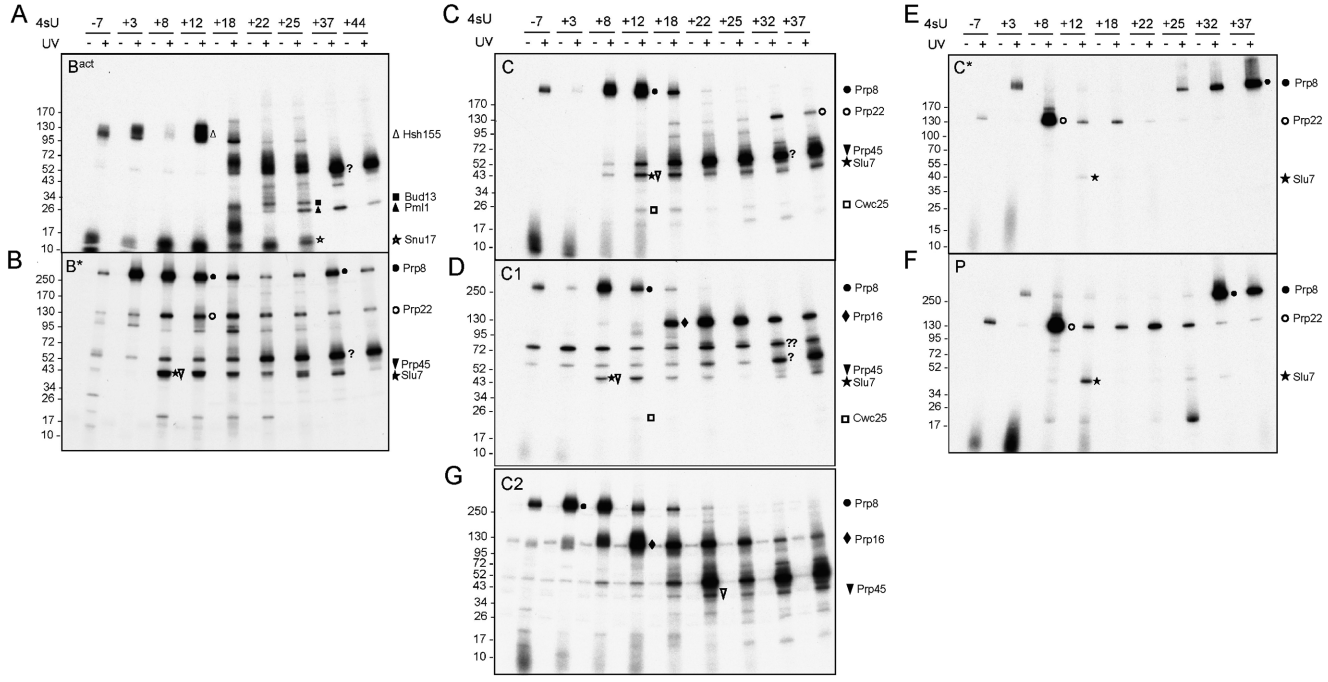

Figure 3. Analysis of total crosslinked proteins at the BS-3′SS region. Splicing was carried out using actin ACAC (A–E) or wild-type pre-mRNA (F and G) with 4sU labeled in the BS-3′SS region at indicated positions in Spp2-depleted Hsh155-HA extracts (**A**), Yju2-depleted extracts (**B**), Prp16-depleted Cwc25-HA extracts (**C**), in the presence of prp16-D473A protein (**D**), in Prp22-V5 extracts (**E** and **G**), in the presence of prp22-S635A-V5 protein (**F**), or in Slu7/Prp22-depleted extracts (G). Following UV-irradiation, the spliceosome was precipitated with anti-HA (A and C), anti-Ntc20 (B and G), anti-Prp16 (D) or anti-V5 (E and F) antibody. Total crosslinked proteins were analyzed on 4–20% gradient SDS-PAGE. Two major crosslinked products of unknown identity are marked as ? (A–D, G) and ?? (D), respectively.

player in mediating the switch. Interestingly, in the absence of Slu7/Prp18/Prp22, strong crosslinking of Prp16 was also observed in the region from the $+8^{BS}$ to $+25^{BS}$ positions (Supplementary Figure S5A), as opposed to from $+18^{BS}$ to $+37^{BS}$ for prp16-D473A (Figure 3D), suggesting movement of Prp16 from its docking site toward the BS under ATP hydrolysis. Without crosslinking, Prp16 was not observed as being stably associated with the spliceosome (Supplementary Figure S5B) unless ATP was depleted prior to immunoprecipitation, indicating that the intermediates could only be captured by crosslinking. The action of Prp16 results in the removal of Cwc25 and Yju2 from the active site of the spliceosome, and possibly also destabilization of the interaction of Prp8 with the BS either directly upon moving close to the BS, or indirectly by removing Cwc25 and Yju2 from the catalytic center.

The fact that Prp8 crosslinked to the intron toward the 3′SS in the C^* and P complexes suggests that the Prp8-interacting site might extend to the 3′-exon. Indeed, Prp8, Slu7 and Prp22 all crosslinked to the 3′-exon in an array both before and after exon ligation (Figure 4 and Supplementary Figure S6). Prp8 crosslinked to positions $+44^{BS}$ and $+51^{BS}$ in both C^* and P complexes, but had an additional crosslink at position $+60^{BS}$ in the P complex. Prp22 had a strong crosslink at position $+60^{BS}$ in the C^* complex, and crosslinking was more evenly distributed from positions $+51^{BS}$ to $+66^{BS}$ in the P complex. Slu7 crosslinking was observed primarily at position $+51^{BS}$ with an additional weaker crosslink at $+60^{BS}$ for the P complex. Together, these results show that Prp8 binds over the 3′SS flanked by Slu7 and Prp22, suggesting that Prp8 plays a central role in positioning the 3′SS during exon ligation, while Slu7/Prp18/Prp22 may promote or stabilize the interaction of Prp8 with the 3′SS.

To establish whether Prp8 interacts with the BS and the 3′SS at different domains, we mapped the crosslinking sites on Prp8 using a TEV-tagged Prp8 system (34). Splicing was carried out in extracts prepared from ZZ-tagged Prp8 strains with a TEV cleavage site inserted at various positions using actin ACAC pre-mRNA labeled with 4sU at the $+8^{BS}$ or $+37^{BS}$ position. Crosslinking at positions $+8^{BS}$ and $+37^{BS}$ was mapped to the same region of Prp8 on the C-terminal half of the linker domain between amino acid residues 1503 and 1673 (Figure 5), which contains the 1585-loop and mutations that affect the first or second reaction (23,44,45). The $+37^{BS}$ position was seen to crosslink to additional sites downstream of the linker domain, possibly in the RH domain (Figure 5C, lane 5). The 1585-loop is located near the catalytic center of the spliceosome in cryo-EM structures (21,25). Our results suggest that the 3′SS is already positioned at the catalytic center in the C^* complex even though the reaction cannot proceed. Furthermore, this segment of Prp8 plays a central role in the alignment of the splice sites for catalysis, whereas Slu7/Prp18/Prp22 play an auxiliary role in the second step.

Identification of proteins crosslinked to the 5′ splice site region

Prp8 has been shown to crosslink to the 5′SS, 3′SS and BS (34,40,46–52), but at which stage of the splicing pathway these interactions occur has not been established. We examined crosslinking at the 5′SS and found that Prp8 crosslinked to the 5′-exon throughout the catalytic phase and predominantly at the $-2^{5'SS}$ position (Figure 6A) (53). This strongly suggests that Prp8 plays a central role in the alignment of the 5′SS and BS in the first step and of the 5′SS and 3′SS in the second step. Snu114, Cwc22 and Cwc21 were seen to crosslink at positions $-20^{5'SS}$ and $-16^{5'SS}$ on the 5′-exon throughout the catalytic phase (Supplementary Figure S7A), in agreement with their observed location near the 5′SS in the cryo-EM structures (21,26,28). At the $-2^{5'SS}$ position, crosslinking of Cwc24 and Prp11 was also detected in the B^{act} complex (53), as was crosslinking of Yju2 in the C complex (Figure 6A and Supplementary Figure S7B), indicating exchange of specific proteins interacting with the 5′SS during the first catalytic step.

A different set of proteins was found to crosslink to the intron sequences of the 5′SS (Figure 6B). As previously reported (54), Cwc2 was seen to crosslink near the 5′SS at the $+9^{5'SS}$ and $+12^{5'SS}$ positions throughout the catalytic phase (Supplementary Figure S8), suggesting a role for Cwc2 in orchestrating the structure of the RNA catalytic center. Several NTC components were found to crosslink to the intron downstream of the 5′SS (Figure 6B, C, Supplementary Figures S9 and S10), supporting a role for the NTC in stabilizing extended U6–5′SS interactions, as suggested previously (4). Interestingly, Ntc30 exhibits strong crosslinking at positions $+9^{5'SS}$ and $+12^{5'SS}$ only in the B^* and C complexes, but also interacts with the intron over a broad sequence expanse further downstream (Figure 6B and C). Ecm2 also interacts with a wide region downstream of the 5′SS, from positions $+20^{5'SS}$ to $+38^{5'SS}$, and more prominently after Prp2-mediated spliceosome remodeling (Figure 6C and Supplementary Figure S11).

A model for positioning the 3′ splice site at the catalytic center of the spliceosome

Based on our crosslinking data, the information from cryo-EM structures (21,22,24–26,28), and previous biochemical analyses (9,10,12,13,55,56), we propose a model for the transition from the first to the second catalytic step as shown in Figure 7. (i) In the first step, Yju2, Cwc25 and Ntc30 (Ntc30 not shown in the figure) are located at the active site, with the cavity surrounded by Prp8 reverse transcriptase (RT), large (L) and RH domains filled by Cwc25, to promote lariat formation (44). Slu7 may interact dynamically with the i3′T (shown by weak interactions of Slu7 with the i3′T). (ii) After branching, Prp16 docks on the intron downstream of the Cwc25 interacting site, and (iii) moves in the 3′ to 5′ direction to remove Cwc25, Yju2 and Ntc30 from the active site, thereby destabilizing the interaction between the Prp8 L domain and the BS. (iv) This action triggers a conformational change in Prp8, allowing rotation of the RH domain and removal of the branch helix from the catalytic site (21,26,28,57). The i3′T can then move freely in the active site until the 3′SS is positioned in the catalytic center. (v) Slu7 can interact with the RH domain in the new position and enter the active site to further interact with the L domain. (vi) When the 3′SS moves into the active site, Slu7 stabilizes its interaction with the 5′SS through simultaneous

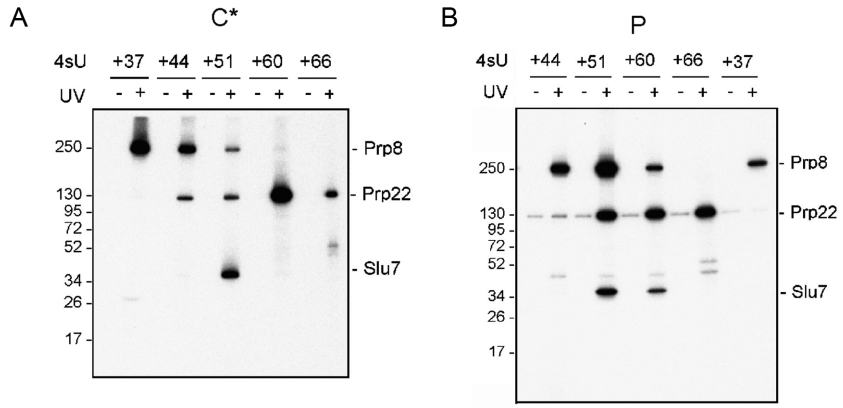

Figure 4. Analysis of total crosslinked proteins in the 3′-exon. Splicing was carried out using actin ACAC (**A**) or wild-type pre-mRNA but in the presence of prp22-S635A-V5 protein (**B**) with 4sU labeled in the 3′-exon region at indicated positions relative to the branchpoint.

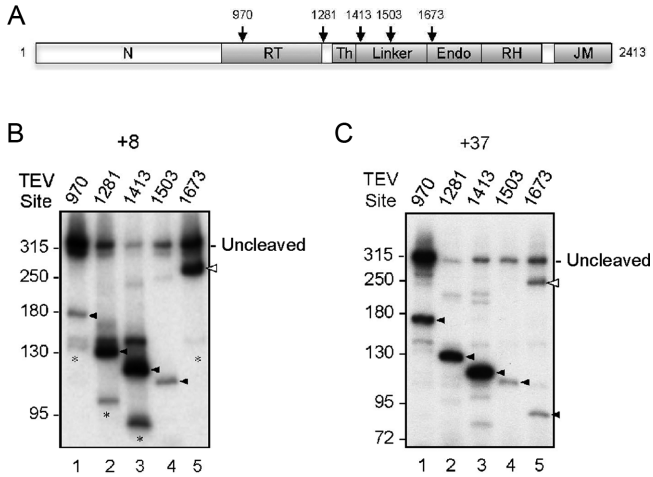

Figure 5. Mapping of Prp8 crosslinked sites. (**A**) A map of Prp8 showing domain organization and TEV insertion sites. (B, C) Spliceosomes were assembled on ACAC pre-mRNA with 4sU labeled at the $+8^{BS}$ (B) or $+37^{BS}$ (C) positions of the BS with (**B**) or without (**C**) the addition of recombinant prp16-D473A, using extracts prepared from strains with the TEV cleavage site inserted at indicated positions of Prp8. Open and filled triangles indicate the N-terminal and C-terminal fragments of Prp8, respectively. *, degraded products.

interactions with exon-2 and Prp8. Prp22 docks on the i3′T, but is unable to get into the active site possibly due to hindrance by the RH domain. Consequently, crosslinking of Prp22 was observed only being close to the $+8^{BS}$ position of the BS. Stalled at the gateway of the cavity, Prp22 interacts with both the i3′T and exon-2. No other proteins were detected to crosslink to the RNA between the two ends of the Prp22-crosslinked sites (Figure 3E). (vii) After exon ligation, the RH domain may rotate away to enlarge the cavity and destabilize the interaction with Slu7, allowing Prp22 to enter and disrupt the interaction between mRNA and Prp8 for the release of mRNA from the spliceosome.

DISCUSSION

By systematic crosslinking analysis using 4sU-labeled pre-mRNA, we have identified protein–RNA interactions at the 5′SS and BS-3′SS regions at defined steps of the catalytic phase of splicing. Splicing was blocked at different stages by depletion of specific factors, addition of dominant-negative Prp16 or Prp22 mutant protein, or using 3′SS mutant ACAC pre-mRNA. Accumulated splicing complexes were then isolated after UV irradiation using antibodies against specific proteins. This resulted in isolation of seven distinct splicing complexes from the catalytic phase, despite whether all of them are true functional intermediates of the spliceosome cannot be concluded. Pre-mRNAs with a single 4sU labeled at 13 positions spreading around the 5′SS and 13 positions around the BS-3′SS region were synthesized for these experiments. The identity of crosslinked proteins was validated by immunoprecipitation of crosslinked products with specific antibodies, but only one or two representative positions from each cluster were analyzed. Although these analyses are not on quantitative basis, they provide an overview on how protein components interact with the splice sites and their surrounding sequences in mediating structural changes of the spliceosome during the two catalytic steps. It is worth noting that each base of pre-mRNA crosslinked to multiple proteins, and each protein crosslinked to multiple RNA residues, suggesting that pre-mRNA interacts with the spliceosome in a rather dynamic manner. This outcome explains why only limited pre-mRNA sequences were detected in cryo-EM structures. Our data revealed that most of the components that interact with the 5′SS, either with the 5′-exon or with the intron, interact with specific regions of the pre-mRNA constitutively throughout the catalytic phase, whereas substantial changes of protein–RNA interactions occur in the BS-3′SS region.

In the cryo-EM structures, the last few bases of the 5′-exon are located between the Prp8 N and L domains that show very little conformational change throughout the catalytic phase. In agreement, we observed Prp8 crosslinked to the $-2^{5'SS}$ to $-16^{5'SS}$ positions on the 5′-exon throughout the catalytic step. The 5′-exon is presumed to extend out through a channel enclosed by Snu114 and the MA3 and MIF4G domains of Cwc22 located on one surface of the spliceosome, but the RNA sequence was not seen (20–22,24,25,28). Consistently, we noted Snu114, Cwc22, Cwc21 and a protein of around 65-kDa of unknown iden-

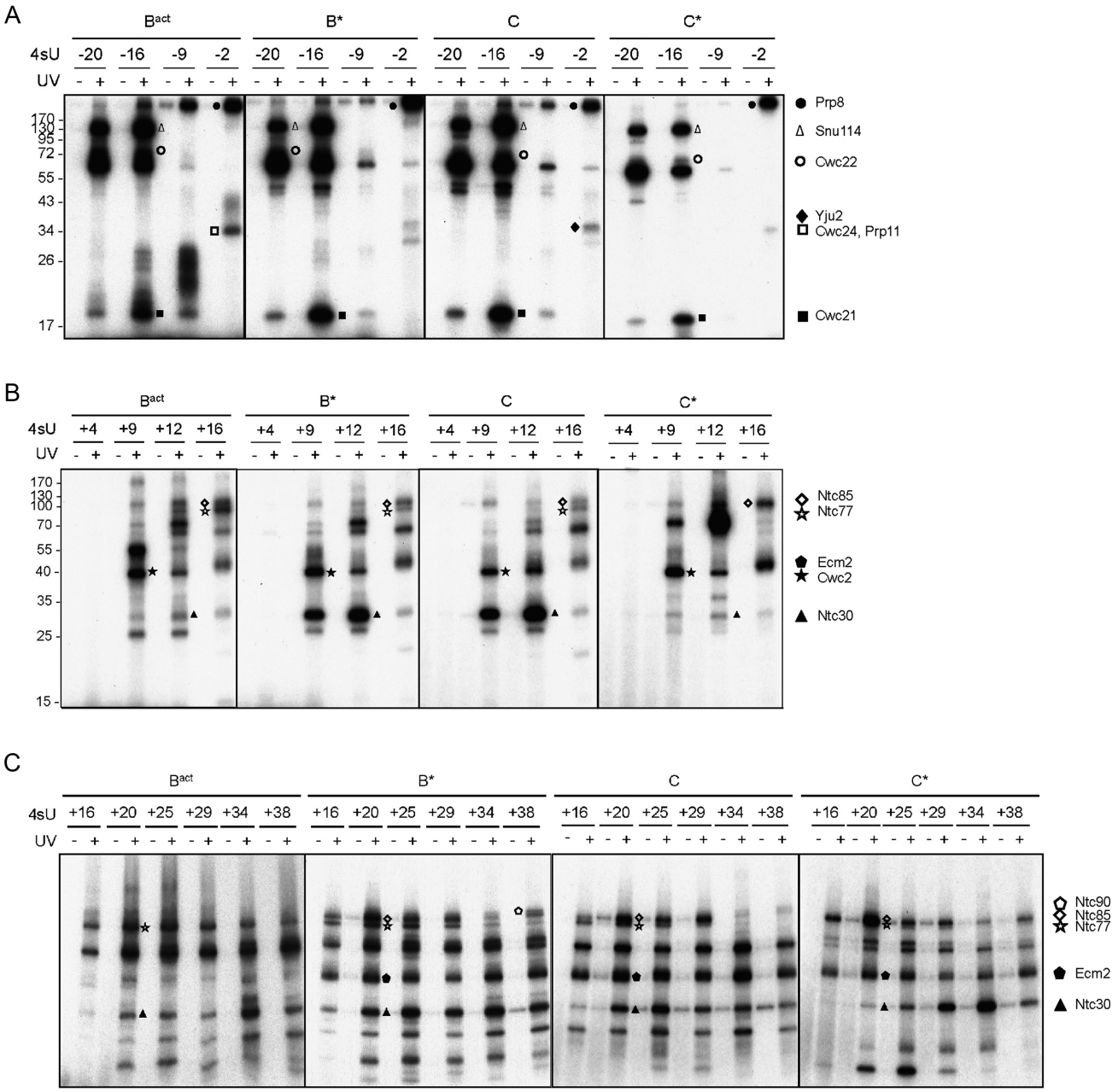

Figure 6. Analysis of total crosslinked proteins at the 5′ splice site. Splicing was carried out using actin ACAC pre-mRNA with 4sU labeled at indicated positions of the 5′-exon (**A**) or intron (**B**, **C**) sequences at the 5′SS in extracts depleted of Spp2 (B^{act}), Yju2 (B^{*}), Prp16 (C), or wild-type extracts (C^{*}). Following UV irradiation, spliceosomes were precipitated with anti-Ntc20 antibody, and analyzed by 12.5% (A) or 4–20% gradient (B, C) SDS-PAGE.

tity crosslinked to the $-16^{5'SS}$ and $-20^{5'SS}$ positions on the 5′-exon. This suggests that the 5′-exon is highly dynamic in this region and can contact any of the four proteins. The 65-kD protein was not seen in cryo-EM structures. It may bind RNA only with low affinity, and can only be detected when crosslinked to RNA. Cwc22 is an eIF4G-like protein, and its human ortholog was shown to interact with the exon-junction-complex (EJC) core component eIF4IIIA for deposition of the EJC on the mRNA for nonsense-mediated mRNA decay (58–60). The position of the Cwc22 crosslinking site conforms with the EJC binding site, supporting its proposed role as an adaptor in recruiting the EJC to the mRNA. In contrast, Cwc24, Prp11 and Yju2 all contact the $-2^{5'SS}$ position of the 5′-exon only at specific stages. They are also only transiently associated with the spliceosome. Cwc24 and Prp11 were detected to crosslink at the $-2^{5'SS}$ position in the B^{act} complex, whereas Yju2 did so in the C complex. In the cryo-EM structures of the B^{act} complex, Cwc24 and Prp11 were observed to interact with the first base of the intron (G1) (20). In agreement, we have detected interactions of Cwc24 with G1 and U2 of the intron by UV-crosslinking, but only weakly with the 5′-exon (53), suggesting that crosslinking using 4sU-labeled pre-mRNA is much

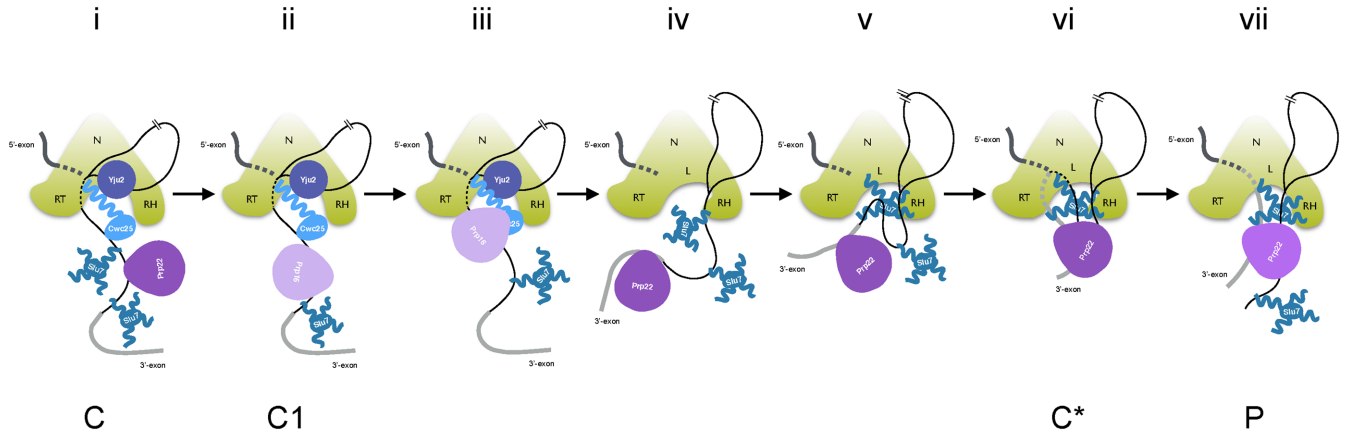

Figure 7. A model for transition from the first to second catalytic step. Domains of Prp8 are shown as follows: N,N-terminal domain; RT, reverse transcriptase domain; L, large domain; RH, RNase H-like domain. Broken lines indicate RNA buried inside Prp8. Black line, intron; dark grey line, 5′-exon; light grey line, 3′-exon.

more efficient than UV-crosslinking. Prp11 has previously been shown to crosslink to the BS upstream region (41), and can interact with both the 5′ SS and BS in the B^{act} complex (20). Prp11 is displaced together with the SF3a/b and RES complexes upon Prp2 action, which presumably disrupts the interactions of SF3a/b and RES with sequences in the BS region. Structural change in the BS region is likely to impact interactions of components at the 5′SS, leading to dissociation of Cwc24.

Proteins crosslinked to the intron sequence near the 5′SS are primarily NTC and NTC-related components. No protein was detected to crosslink to the $+4^{5'SS}$ position of the intron, possibly due to base pairing of the residue with U6 snRNA after spliceosome activation. Cwc2 was previously shown to contact the $+15^{5'SS}$ position by UV-crosslinking (54). We observed crosslinking of Cwc2 at positions even closer to the 5′SS, i.e. at positions $+9^{5'SS}$ and $+12^{5'SS}$, suggesting that Cwc2 may play a critical role in supporting the structure of the catalytic center of the spliceosome. Isy1/Ntc30 also showed strong crosslinking at positions $+9^{5'SS}$ and $+12^{5'SS}$ in the B^* and C complexes of the first step. Consistently, the N-terminal region of Ntc30 was detected at the catalytic center of the spliceosome in the cryo-EM structure of the C complex (22,25). Although Ntc30 is not seen in any other cryo-EM structures, our results demonstrate that, like other NTC components, Ntc30 also interacts with a broad range of the intron sequences downstream of the 5′SS throughout the catalytic phase. This finding suggests that Ntc30 may interact with the spliceosome in a dynamic manner, and its N-terminal domain is stabilized when positioned close to the active site during the first step. Syf1/Ntc90, Cef1/Ntc85, Clf1/Ntc77 and Ecm2 were found to crosslink to positions $+16^{5'SS}$ to $+38^{5'SS}$ of the intron sequence, with this region previously having been shown to interact with the Lsm-binding site of U6 snRNA in an NTC-dependent manner (4). On binding to the 5′SS downstream region, NTC components may promote the release of the Lsm complex from U6 and further stabilize the interaction of the pre-mRNA with the U6 3′ tail. Whether NTC components also directly interact with U6 snRNA remains to be investigated.

Crosslinking in the i3′T region also underwent a major change after Prp2-mediated remodeling of the spliceosome. Prp8 replaces Hsh155 to interact with the BS upon the release of SF3a/b, and remains bound until Yju2 and Cwc25 are displaced after the first reaction. Prp8 then binds to the 3′SS while retaining interaction with the 5′-exon for exon ligation. These results suggest that the Prp8 protein plays a key role in positioning the 5′SS and the BS for lariat formation, and the 5′SS and 3′SS for exon ligation. Mapping of crosslinked sites identified a region of Prp8 between amino acid residues 1503 and 1673 in the linker domain that crosslinked to the $+8^{BS}$ position of the C1 complex and to the $+37^{BS}$ position of the C^* complex. This region contains the 1585-loop located at the catalytic center of the spliceosome. This finding indicates that the BS and the 3′SS are positioned at the catalytic center of the C1 and C^* complexes, respectively, and it is consistent with observations based on cryo-EM structures of the spliceosome C^* complex, which show that the branch helix is oriented away from the catalytic center by 60 Å and that an RNA fragment, likely containing the 3′SS and the 3′-exon sequences, is located at the catalytic center. An additional crosslinked site toward the C-terminal end of Prp8, possibly in the RH-domain, was also seen for the $+37^{BS}$ position, presumably arising from the population of spliceosomes whose 3′SS had not yet been positioned at the catalytic center. These results suggest that during the second step, Prp16 mediates remodeling of the spliceosome not only to remove Yju2 and Cwc25 from the active site but also to destabilize the interaction of Prp8 with the BS, allowing the 3′SS to displace the BS for interaction with Prp8.

Prp16 was seen to crosslink to the i3′T from position $+18^{BS}$ to the 3′SS when the dominant-negative ATPase mutant D473A was used in the splicing reaction. Similarly, the Prp2 helicase mutant S378L could crosslink to the i3′T in the same region of pre-mRNA, but requires more than 20 nt downstream of the branchpoint for crosslinking (61). Both Prp2 and Prp16 interact with the C-terminal domain of Brr2, which has been shown to interact with many spliceosomal components, and might serve as the platform for recruiting proteins to the spliceosome (62). Prp2 was pro-

posed to first interact with Brr2, and then to translocate to the i3′T of the pre-mRNA. Upon ATP hydrolysis, Prp2 can move in the 3′ to 5′ direction to displace SF3a/b (61). Conceivably, Prp16 may act in a similar way to displace Yju2 and Cwc25 from the active site. Supporting this notion, our data show that when splicing was performed in Slu7-depleted extracts, wild-type Prp16 could crosslink to a region of the i3′T much closer to the BS than could the D473A mutant, implicating ATP hydrolysis-driven movement of Prp16 from its docking site toward the BS. Moreover, the Prp16 crosslinked sites overlap with those of Prp8 near the BS. This result suggests that Prp16 may displace the Prp8-i3′T interaction on moving toward the BS, which then allows the 3′SS to enter the active site to interact with Prp8. Nevertheless, without crosslinking, Prp16 was not detected to associate with the spliceosome by immunoprecipitation unless ATP was depleted from the reaction mixture prior to immunoprecipitation, suggesting that Prp16 only weakly interacts with the spliceosome during cycles of ATP hydrolysis.

Both Slu7 and Prp22 interact with the i3′T near the BS at earlier stages before their functions are required. Crosslinking was detected as early as in the B^* complex after Prp2-mediated remodeling of the spliceosome. Slu7 has previously been shown to facilitate the release of Yju2 and Cwc25 after the first reaction (55), consistent with its early association with the spliceosome. Slu7 interacts with the i3′T throughout the catalytic phase, with crosslinks also detected in the P complex. Judging from its weak but broad-range crosslinking, Slu7 might interact with the i3′T nonspecifically. In contrast, a strong crosslink of Slu7 at position $+51^{BS}$ was observed in the C^* complex, accompanied by switching of Prp8 crosslinking from the BS to the 3′SS. This finding suggests that Slu7 might interact strongly with the 3′-exon after Prp16-mediated spliceosome remodeling. Slu7 was seen to interact with the N, linker and RH domains of Prp8 in the cryo-EM structures of the C^* complex, but not seen in those of the C complex (19,21,27–30), suggesting that Slu7 is not stably associated with the spliceosome before formation of the C^* complex. Since Slu7 is required for switching the Prp8 crosslinking site, the interaction of Slu7 with the 3′-exon and/or with Prp8 might be important for the switch. It is conceivable that Slu7 may access the spliceosome through dynamic interactions with pre-mRNA sequences downstream of the BS to prepare for docking to the spliceosome. When the branch helix is moved away from the active site, the i3′T and Slu7 can enter the active site, allowing Slu7 to be deposited on the spliceosome upon interacting with Prp8. This may facilitate the interaction of Slu7 with the 3′-exon to promote or stabilize the interaction of Prp8 with the 3′SS.

Crosslinks of Prp8 to the BS region were observed primarily at positions $+8^{BS}$ to $+12^{BS}$. A strong crosslink at the $+3^{BS}$ position was also seen, but only in the B^* and C2 complexes, which represent the spliceosome arrested at stages after SF3a/b and Yju2/Cwc25, respectively, are displaced. The crosslinked site on Prp8 was mapped to the same region containing the 1585-loop that crosslinks to positions $+8^{BS}$ and $+37^{BS}$ (data not shown). Conceivably, removing SF3a/b and Yju2/Cwc25 from the active site could create an open space at the catalytic center of the spliceosome, allowing the branch helix to move more freely into the active site in the case of the B^* complex or to exit it for the C2 complex. This scenario would also enable the $+3^{BS}$ residue to interact with Prp8. The presence of SF3a/b or Yju2/Cwc25 likely prevents $+3^{BS}$ from interacting with Prp8 by sequestering the two elements or by restraining the conformation of the active site. Cryo-EM structures of the B^{act} complex indeed reveal sequestering of the branch helix from the catalytic center by Hsh155/SF3b1 (20,24). In contrast, the branch helix is located at the active site with $+3^{BS}$ positioned close to but not in contact with Prp8 in the cryo-EM structures of the C complex (22,25), suggesting that the active site of the spliceosome is structurally inflexible and prohibits free movement of the pre-mRNA.

Although cryo-EM structures of the spliceosome reveal detailed arrangements and interactions of the spliceosomal components, very little of the pre-mRNA sequences was observable due to the dynamic character of the pre-mRNA in these structures. How spliceosomal components interact with the pre-mRNA is not well elucidated, except for those at the conserved splice site sequences. By site-specific crosslinking analysis, we were able to visualize interactions of protein components with the pre-mRNA in the 5′SS, 3′SS and BS regions at various stages of the catalytic phase, even under conditions when the interactions are more dynamic, such as the interaction of Slu7, Prp22 and Prp16 with the i3′T. It is particularly valuable to reveal the interactions of those complexes in open conformational states (63), such as the B^* and C2 complexes, whose dynamic nature at the active site would make structural determination difficult.

SUPPLEMENTARY DATA

Supplementary Data are available at NAR Online.

ACKNOWLEDGEMENTS

We thank K. Nagai and P.-C. Lin for careful comments on the manuscript. We also thank H.-T. Chen for the kind gift of TEV protease, J. O'Brien for English editing, and members of the Cheng laboratory for helpful discussions.

FUNDING

Academia Sinica and the Minister of Science and Technology (Taiwan) [MoST106–2321-B-001-007]. Funding for open access charge: Ministry of Science and Technology, Taiwan.
Conflict of interest statement. None declared.

REFERENCE

1. Brow,D.A. (2002) Allosteric cascade of spliceosome activation. *Annu. Rev. Genet.*, **36**, 333–360.
2. Wahl,M.C., Will,C.L. and Lührmann,R. (2009) The spliceosome: design principles of a dynamic RNP machine. *Cell,* **136**, 701–718.
3. Will,C.L. and Lührmann,R. (2011) In: Atkins,JFRFG and Cech,TR (ed). *Cold Spring Harb. Perspect. Biol*. Cold Spring Harbor Laboratory Press, NY, Vol. **3**, p. a003707.
4. Chan,S.-P., Kao,D.-I., Tsai,W.-Y. and Cheng,S.-C. (2003) The Prp19p-associated complex in spliceosome activation. *Science*, **302**, 279–282.

5. Tarn,W.-Y., Lee,K.-R. and Cheng,S.-C. (1993a) The yeast PRP19 protein is not tightly associated with small nuclear RNAs, but appears to associate with the spliceosome after binding of U2 to the pre-mRNA and prior to formation of the functional spliceosome. *Mol. Cell. Biol.*, **13**, 1883–1891.
6. Tarn,W.-Y., Lee,K.-R. and Cheng,S.-C. (1993b) Yeast precursor mRNA processing protein PRP19 associates with the spliceosome concomitant with or just after dissociation of U4 small nuclear RNA. *Proc. Natl. Acad. Sci. U.S.A.*, **90**, 10821–10825.
7. Staley,J.P. and Guthrie,C. (1998) Mechanical devices of the spliceosome: motors, clocks, springs, and things. *Cell*, **92**, 315–326.
8. Linder,P. and Jankowsky,E. (2011) From unwinding to clamping - the DEAD box RNA helicase family. *Nat. Rev. Mol. Cell Biol.*, **12**, 505–516.
9. Warkocki,Z., Odenwälder,P., Schmitzová,J., Platzmann,F., Stark,H., Urlaub,H., Ficner,R., Fabrizio,P. and Lührmann,R. (2009) Reconstitution of both steps of Saccharomyces cerevisiae splicing with purified spliceosomal components. *Nat. Struct. Mol. Biol.*, **16**, 1237–1243.
10. Lardelli,R.M., Thompson,J.X., Yates,J.R. III and Stevens,S.W. (2010) Release of SF3 from the intron branchpoint activates the first step of pre-mRNA splicing. *RNA*, **16**, 516–528.
11. Chiu,Y.-F., Liu,Y.-C., Chiang,T.-W., Yeh,T.-C., Tseng,C.-K., Wu,N.Y. and Cheng,S.-C. (2009) Cwc25 is a novel splicing factor required after Prp2 and Yju2 to facilitate the first catalytic reaction. *Mol. Cell. Biol.*, **29**, 5671–5678.
12. Tseng,C.-K., Liu,H.-L. and Cheng,S.-C. (2011) DEAH-box ATPase Prp16 has dual roles in remodeling of the spliceosome in catalytic steps. *RNA*, **17**, 145–154.
13. Liu,Y.-C., Chen,H.-C., Wu,N.-Y. and Cheng,S.-C. (2007) A novel splicing factor Yju2 is associated with NTC and acts after Prp2 in promoting the first catalytic reaction of pre-mRNA splicing. *Mol. Cell. Biol.*, **27**, 5403–5413.
14. Company,M., Arenas,J. and Abelson,J. (1991) Requirement of the RNA helicase-like protein PRP22 for release of messenger RNA from spliceosomes. *Nature*, **349**, 487–493.
15. Tsai,R.-T., Fu,R.-H., Yeh,F.-L., Tseng,C.-K., Lin,Y.-C., Huang,Y.-H. and Cheng,S.-C. (2005) Spliceosome disassembly catalyzed by Prp43 and its associated components Ntr1 and Ntr2. *Genes Dev.*, **19**, 2991–3003.
16. Arenas,J.E. and Abelson,J.N. (1997) Prp43: An RNA helicase-like factor involved in spliceosome disassembly. *Proc. Natl. Acad. Sci. U.S.A.*, **94**, 11798–11802.
17. Martin,A., Schneider,S. and Schwer,B. (2002) Prp43 is an essential RNA-dependent ATPase required for release of lariat-intron from the spliceosome. *J. Biol. Chem.*, **277**, 17743–17750.
18. Su,Y.-L., Chen,H.-C., Tsai,R.-T., Lin,P.-C. and Cheng,S.-C. (2018) Cwc23 is a component of the NTR complex and functions to stabilize Ntr1 and facilitate disassembly of spliceosome intermediates. *Nucleic Acids Res.*, **46**, 3764–3773.
19. Bai,R., Yan,C., Wan,R., Lei,J. and Shi,Y. (2017) Structure of the post-catalytic spliceosome from Saccharomyces cerevisiae. *Cell,* **171**, 1589–1598.
20. Yan,C., Wan,R., Bai,R., Huang,G. and Shi,Y. (2016) Structure of a yeast activated spliceosome at 3.5-Å resolution. *Science*, **353**, 904–911.
21. Yan,C., Wan,R., Bai,R., Huang,G. and Shi,Y. (2017) Structure of a yeast step II catalytically activated spliceosome. *Science*, **355**, 149–155.
22. Wan,R., Yan,C., Bai,R., Huang,G. and Shi,Y. (2016) Structure of a yeast catalytic step I spliceosome at 3.4 Å resolution. *Science*, **353**, 895–904.
23. Wan,R., Yan,C., Bai,R., Wang,L., Huang,M., Wong,C.C.L. and Shi,Y. (2016) The 3.8 Å structure of the U4/U6.U5 tri-snRNP: Insights into spliceosome assembly and catalysis. *Science*, **351**, 466–475.
24. Rauhut,R., Fabrizio,P., Dybkov,O., Hartmuth,K., Pena,V., Chari,A., Kumar,V., Lee,C.-T., Urlaub,H., Kastner,B. *et al.* (2016) Molecular architecture of the Saccharomyces cerevisiae activated spliceosome. *Science*, **353**, 1399–1405.
25. Galej,W.P., Wilkinson,M.E., Fica,S.M., Oubridge,C., Newman,A.J. and Nagai,K. (2016) cryo-EM structure of the spliceosome immediately after branching. *Nature*, **537**, 197–201.
26. Bertram,K., Agafonov,D.E., Liu,W.-T., Dybkov,O., Will,C.L., Hartmuth,K., Urlaub,H., Kastner,B., Stark,H. and Lührmann,R. (2017) Cryo-EM structure of a human spliceosome activated for step 2 of splicing. *Nature*, **542**, 318–323.
27. Zhang,X., Yan,C., Hang,J., Finci,L.I., Lei,J. and Shi,Y. (2017) An atomic structure of the human spliceosome. *Cell*, **169**, 918–929.
28. Fica,S.M., Oubridge,C., Galej,W.P., Wilkinson,M.E., Bai,X.-C., Newman,A.J. and Nagai,K. (2017) Structure of a spliceosome remodeled for exon ligation. *Nature*, **542**, 377–380.
29. Wilkinson,M.E., Fica,S.M., Galej,W.P., Norman,C.M., Newman,A.J. and Nagai,K. (2017) Postcatalytic spliceosome structure reveals mechanism of 3′-splice site selection. *Science*, **358**, 1283–1288.
30. Liu,S., Li,X., Zhang,L., Jiang,J., Hill,R.C., Cui,Y., Hansen,K.C., Zhou,Z.H. and Zhao,R. (2017) Structure of the yeast spliceosomal postcatalytic P complex. *Science*, **358**, 1278–1283.
31. Bai,R., Wan,R., Yan,C., Lei,J. and Shi,Y. (2018) Structures of the fully assembled Saccharomyces cerevisiae spliceosomes before activation. *Science*, **360**, 1423–1429.
32. Cheng,S.-C., Newman,A., Lin,R.-J., McFarland,G.D. and Abelson,J.N. (1990) Preparation and fractionation of yeast splicing extract. *Methods Enzymol.*, **181**, 89–96.
33. Sontheimer,E.J. (1994) Site-specific RNA crosslinking with 4-thiouridine. *Mol. Biol. Rep.*, **20**, 35–44.
34. Turner,I.A., Norman,C.M., Churcher,M.F. and Newman,A.J. (2006) Dissection of Prp8 protein defines multiple interactions with crucial RNA sequences in the catalytic core of the spliceosome. *RNA*, **12**, 375–386.
35. Hotz,H.-R. and Schwer,B. (1998) Mutational analysis of the yeast DEAH-box splicing factor Prp16. *Genetics*, **149**, 807–815.
36. Schwer,B. and Meszaros,T. (2000) RNA helicase dynamics in pre-mRNA splicing. *EMBO J.*, **19**, 6582–6591.
37. Schneider,S., Hotz,H.-R. and Schwer,B. (2002) Characterization of dominant-negative mutants of the DEAH-box splicing factors Prp22 and Prp16. *J. Biol. Chem.*, **277**, 15452–15458.
38. Tseng,C.-K. and Cheng,S.-C. (2008) Both catalytic steps of nuclear pre-mRNA splicing are reversible. *Science*, **320**, 1782–1784.
39. Gozani,O., Potashkin,J. and Reed,R. (1998) A potential role for U2AF SAP155 interactions in recruiting U2 snRNP to the branch site. *Mol. Cell. Biol.*, **18**, 4752–4760.
40. McPheeters,D.S. and Muhlenkamp,P. (2003) Spatial organization of protein–RNA interactions in the branch site-3′ splice site region during pre-mRNA splicing in yeast. *Mol. Cell. Biol.*, **23**, 4174–4186.
41. Schneider,C., Agafonov,D.E., Schmitzová,J., Hartmuth,K., Fabrizio,P. and Lührmann,R. (2015) Dynamic contacts of U2, RES, Cwc25, Prp8 and prp45 proteins with the pre-mRNA branch-site and 3′ splice site during catalytic activation and step 1 catalysis in yeast spliceosomes. *PLoS Genet.*, **11**, e1005539.
42. Chen,H.-C., Tseng,C.-K., Tsai,R.-T., Chung,C.-S. and Cheng,S.-C. (2013) Link of NTR-mediated spliceosome disassembly with DEAH-box ATPases Prp2, Prp16 and Prp22. *Mol. Cell. Biol.*, **33**, 514–525.
43. Schwer,B. (2008) A conformational rearrangement in the spliceosome sets the stage for Prp22-dependent mRNA release. *Mol. Cell*, **30**, 743–754.
44. Galej,W.P., Oubridge,C., Newman,A.J. and Nagai,K. (2013) Crystal structure of Prp8 reveals active site cavity of the spliceosome. *Nature*, **493**, 638–643.
45. Liu,L., Query,C.C. and Konarska,M.M. (2007) Opposing classes of prp8 alleles modulate the transition between the catalytic steps of pre-mRNA splicing. *Nat. Struct. Mol. Biol.*, **14**, 519–526.
46. Wyatt,J.R., Sontheimer,E.J. and Steitz,J.A. (1992) Site-specific cross-linking of mammalian U5 snRNP to the 5′ splice site before the first step of pre-mRNA splicing. *Genes Dev.*, **6**, 2542–2553.
47. Teigelkamp,S., Newman,A.J. and Beggs,J.D. (1995) Extensive interactions of PRP8 protein with the 5’ and 3’ splice sites during splicing suggest a role in stabilization of exon alignment by U5 snRNA. *EMBO J.*, **14**, 2602–2612.
48. Umen,J.G. and Guthrie,C. (1995) Prp16p, Slu7p and Prp8p interact with the 3’ splice site in two distinct stages during the second catalytic step of pre-mRNA splicing. *RNA*, **1**, 584–597.
49. Chiara,M.D., Gozani,O., Bennett,M., Champion-Arnaud,P., Palandjian,L. and Reed,R. (1996) Identification of proteins that interact with exon sequences, splice sites, and the branchpoint

sequence during each stage of spliceosome assembly. *Mol. Cell. Biol.*, **16**, 3317–3326.
50. Reyes,J.L., Gustafson,E.H., Moore,M.J. and Konarska,M.M. (1999) The C-terminal region of hPrp8 interacts with the conserved GU dinucleotide at the 5′ splice site. *RNA*, **5**, 167–179.
51. Reyes,J.L., Kois,P., Konforti,B.B. and Konarska,M.M. (1996) The canonical GU dinucleotide at the 5′ splice site is recognized by p220 of the U5 snRNP within the spliceosome. *RNA*, **2**, 213–225.
52. Maroney,P.A., Romfo,C.M. and Nilsen,T.W. (2000) Functional recognition of the 5' splice site by U4/U6.U5 tri-snRNP defines a novel ATP-dependent step in early spliceosome assembly. *Mol. Cell*, **6**, 317–328.
53. Wu,N.-Y., Chung,C.-S. and Cheng,S.-C. (2017) Roles of Cwc24 in the first catalytic step and fidelity in 5′ splice site selection. *Mol. Cell. Biol.*, **37**, e00580-16.
54. Rasche,N., Dybkov,O., Schmitzová,J., Akyildiz,B., Fabrizio,P. and Lührmann,L. (2012) Cwc2 and its human homologue RBM22 promote an active conformation of the spliceosome catalytic centre. *EMBO J.*, **31**, 1591–1604.
55. Ohrt,T., Odenwalder,P., Dannenberg,J., Prior,M., Warkocki,Z., Schmitzova,J., Karaduman,R., Gregor,I., Enderlein,J., Fabrizio,P. *et al.* (2013) Molecular dissection of step 2 catalysis of yeast pre-mRNA splicing investigated in a purified system. *RNA*, **19**, 902–915.
56. Semlow,D.R., Blanco,M.R., Walter,N.G. and Staley,J.P. (2016) Spliceosomeal DEAH-box ATPase remodel pre-mRNA to activate alternative splice sites. *Cell*, **164**, 985–998.
57. Abelson,J. (2017) A close-up look at the spliceosome, at last. *Proc. Natl. Acad. Sci. U.S.A.*, **114**, 4288–4293.
58. Alexandrov,A., Colognori,D., Shu,M.-D. and Steitz,J.A. (2012) Human spliceosomal protein CWC22 plays a role in coupling splicing to exon junction complex deposition and nonsense-mediated decay. *Proc. Natl. Acad. Sci. U.S.A.*, **109**, 21313–21318.
59. Barbosa,I., Haque,N., Fiorini,F., Barrandon,C., Tomasetto,C., Blanchette,M. and Le Hir,H. (2012) Human CWC22 escorts the helicase eIF4AIII to spliceosomes and promotes exon junction complex assembly. *Nat. Struct. Mol. Biol.*, **19**, 983–991.
60. Steckelberg,A.L., Boehm,V., Gromadzka,A.M. and Gehring,N.H. (2012) CWC22 connects pre-mRNA splicing and exon junction complex assembly. *Cell Rep.*, **2**, 454–461.
61. Liu,H.-L. and Cheng,S.-C. (2012) The interaction of Prp2 with a defined region of the intron is required for the first splicing reaction. *Mol. Cell. Biol.*, **32**, 5056–5066.
62. van Nues,R.W. and Beggs,J.D. (2001) Functional contacts with a range of splicing proteins suggest a central role for Brr2p in the dynamic control of the order of events in spliceosomes of Saccharomyces cerevisiae. *Genetics*, **157**, 1451–1467.
63. Tseng,C.-K., Chung,C.-S., Chen,H.-C. and Cheng,S.-C. (2017) A central role of Cwc25 in spliceosome dynamics during catalytic phase of pre-mRNA splicing. *RNA*, **23**, 546–556.